Electrophoretic deposition of composite coatings based on alginate matrix/45S5 bioactive glass particles doped with B, Zn or Sr

Electrophoretic deposition of composite coatings based on alginate matrix/45S5 bioactive glass particles doped with B, Zn and Sr

Marta Miola[1]*, Luis Cordero-Arias[2,3], Giulia Ferlenda[1,6], Andrea Cochis[4], Sannakaisa Virtanen[5], Lia Rimondini[4], Enrica Verné[1], Aldo R. Boccaccini[2]

[1] *Institute of Materials Physics and Engineering, Department of Applied Science and Technology, Politecnico di Torino - POLITO, Italy*

[2] *Institute of Biomaterials, University of Erlangen-Nuremberg, 91058 Erlangen, Germany*

[3] *Escuela de Ciencia e Ingeniería de los Materiales, Instituto Tecnológico de Costa Rica, Campus Central Cartago, Costa Rica*

[4] *Department of Health Sciences, Center for Translational Research on Autoimmune and Allergic Diseases–CAAD, Università del Piemonte Orientale - UPO, Novara, Italy*

[5] *Institute of Surface Science and Corrosion, University of Erlangen-Nuremberg, 91058 Erlangen, Germany*

[6] *Gealpharma, Bricherasio (TO), Italy*

**Corresponding author: marta.miola@polito.it*

Politecnico di Torino

Department of Applied Science and Technology, Politecnico di Torino, Torino (TO), Italy

Institute of Materials Engineering and Physics

Corso Duca degli Abruzzi, 24 - 10129 (TORINO) ITALY

Tel: +39 0110904717

Fax: +39 011 0904624

Abstract

In this research work composite coatings made of alginate and 45S5 bioactive glass particles doped with B, Zn and Sr were synthesized by means of electrophoretic deposition and characterized from morphological, compositional, thermogravimetric, mechanical and electrochemical point of view. The developed coatings were also subjected to *in vitro* test in SBF solution to evaluate their ability to induce hydroxyapatite precipitation and cytocompatibility evaluation using human primary fibroblasts.

The obtained results demonstrated a good homogeneity of the coatings, high adhesion and a protective behavior towards the substrate. The thermogravimetric analysis proved that the glass amount is constant before and after the deposition and all the investigated coatings promoted the deposition of hydroxyapatite but with different kinetics. Since the Zn containing coating show the best bioactive behavior it was subjected to cytocompatibility test, which demonstrated, after an initial reduction of cell viability, a good cells proliferation and the production of collagen from the ECM. These findings suggest that the obtained coatings are promising materials to coat prosthetic devices.

Keywords

Bioactive glasses, alginate, electrophoretic deposition, composite coatings

Introduction

In recent years, electrophoretic deposition (EPD) has been widely explored for a variety of applications in biomaterials science [1]. In particular, EPD has been successfully adopted a simple and powerful method to coat metal substrates (e.g. stainless steel, titanium based alloys, etc.), including composite coatings made of mixtures of polymeric and bioactive inorganic phases, aiming to promote their applications as bone implants [2]. Among bioactive materials, bioactive glasses (BGs) have been successfully used as dispersed bioactive phase into EPD composite coatings [3-7]. BGs are well known for their ability to react with biological fluids, promoting the crystallization of hydroxyapatite (HAp) on their surface and their bone integration *in vivo* [8, 9]. Moreover, the composition of BGs can be tuned by doping with a variety of elements, to impart specific supplementary properties to the implant, such as enhanced osseointegration, antibacterial or angiogenetic effects [10]. In this scenario, several research groups have developed innovative BGs doped with beneficial ions, to design new biomaterials for regenerative medicine [10]. Among them, boron (B), zinc (Zn) and strontium (Sr) attracted great interest for a variety of beneficial effects, such as wound healing stimulation *in vivo,* protein synthesis activation in osteoblasts, upregulation of the extracellular matrix turnover and for their role in angiogenesis [10-16].

Alginate is a natural polysaccharide characterized by exceptional biocompatibility, biodegradability and easiness of gelation. Owing to its processability and structural similarity to the extracellular matrix, alginate has been particularly attractive for many applications in biomedical science and engineering. For example, in the development of three-dimensional scaffolds (hydrogels, microcapsules, microspheres, foams and fibers) which have been employed as drug delivery systems, cell carriers for tissue engineering and wound healing [17, 18], as well as matrix for EPD composite coatings [6, 7].

In this contest, the purpose of the present research work is to explore the feasibility of electrophoretic deposition of composite coatings made of alginate matrix embedding 45S5 bioactive glass particles doped with B, Zn and Sr, and to characterize them in terms of adhesion, morphology and composition. The effect of doping elements on coatings bioactivity and cytocompatibility was evaluated aiming to investigate the opportunity of their application for bone implant applications.

1. Experimental

1.1. Preparation of the glass/polymer suspension

Three different bioactive glasses have been developed starting from the base composition of Bioglass®, 45S5. In particular, 6 mol % of ZnO and SrO have been added in substitution of CaO (namely, 45S5_Zn and 45S5_Sr,

respectively) and 3 % of B_2O_3 have been added in substitution of SiO_2+P_2O_5 (45S5_B). Table 1 reports the glass compositions compared with that of Bioglass 45S5®.

Compound	Bioactive glass type (composition in wt.%)		
	45S5_Sr	**45S5_Zn**	**45S5_B**
SiO_2	43.01	43.92	43.50
Na_2O	23.42	23.91	24.50
P_2O_5	5.73	5.86	4.50
CaO	18.19	18.58	24.50
SrO	9.65	0.00	0.00
ZnO	0.00	7.74	0.00
B_2O_3	0.00	0.00	3.00

Table 1: Chemical composition of the three bioactive glasses developed by doping 45S5 with B, Sr, or Zn.

The glasses have been produced by melt and quenching route. Reagent grade precursors have been mixed and thermally treated in a platinum crucible at 1500 °C for 30 min until melting. The melt has been poured in water obtaining a frit, air dried at room temperature overnight and subsequently milled in a ZrO_2 6-ball planetary mill (Fritsch, Pulverisette 6) and sieved to a grain size < 20 μm. All glasses were characterized in terms of structure, morphology, composition and *in vitro* reactivity, as reported in [4, 5].

A suspension of glass particles in alginate has been prepared as follows. A stock solution of sodium alginate (W201502 Sigma Aldrich) was prepared by dissolving the sodium alginate in deionized water (Purelab Option R7BP, ELGA) under magnetic stirring and subsequent sonication (Bandelin Sonorex, Germany). Ethanol (VWR) was added to reach different water/ethanol proportions (i.e. 20, 40, 60 and 80 vol.%). Ethanol is used to avoid water hydrolysis during EPD and the subsequent bubble formation and accumulation in the final coating. For all the different water-ethanol mixtures, the final alginate concentration was 2 g/L. Glass powders have been added to 50 ml of the different water-ethanol solutions, to prepare suspensions of 6 g/L for each glass composition. To produce a stable and homogeneous suspension, magnetic stirring and subsequent sonication were used. Under these conditions an optimal polymer/glass ratio of 1:3 was reached, as previously observed [7]. In order to optimize the stability of the colloidal suspension and to assess the correct

water/ethanol ratio, the zeta potential measurement has been performed (Zetasizer nano ZS, Malvern Instrument, UK). For each measurement, a glass particle concentration of 0.1 g/L has been used, by diluting the original suspension while maintaining constant the polymer/glass particle ratio and the water-ethanol proportions.

1.2 Electrophoretic deposition

Before each deposition process, the suspension has been magnetically stirred to prevent particle sedimentation and coagulation. EPD coatings have been deposited on stainless steel AISI 316L substrates (30x15 mm deposition area and 0.2 mm thickness of the stainless steel foils) with a stainless steel counter electrode. The distance between the electrodes was fixed to 10 mm. Different times of deposition (from 5 seconds to 3 minutes) and potentials (from 5 to 50 V) have been used in order to determine the best deposition parameters. After the deposition, the coated stainless steel substrates were removed from the solution, rinsed in distilled water and dried at room temperature for 24 hours previous further characterization.

1.3 Morphological, compositional and mechanical characterization

The adhesion of the coatings has been qualitatively evaluated by bending test, that consisted in bending each sample up 180° and evaluating the eventual detachment of the coating from the substrate by optical microscopy. The coating morphology and composition have been observed by optical microscopy (M50, Leica) and by scanning electron microscopy (SEM Carl Zeiss Auriga with EDS, X-MaxN Oxford Instruments, UK). The wettability of the coatings has been evaluated by measuring the surface static contact angle by the sessile drop method (Misura, Expert System Solution). The measure has been carried out by depositing a drop (5 μl) of bi-distilled water on the sample surface and recording the shape by a camera. Subsequently, the obtained images have been analyzed by Image J software (1.47 version). The presented values are an average of three measurements.

Fourier Transform Infrared Spectroscopy (FTIR - Nicolet 6700, Massachusetts, United States) has been carried out to identify the characteristic chemical groups of both alginate and bioactive glass and thus to verify their presence in the coating. The FTIR analysis has been performed on pellets obtained by mixing 200 mg of KBr with 2 mg of coating material manually detached from the substrate. The mixture has been previously manually mixed in a mortar and then pressed in a mold under a force of 10^5 N.

1.4 Thermogravimetric analysis

In order to evaluate the variation of the sample weight as function of temperature and to determine the real amount of glass in the coatings, thermogravimetric analysis (TGA) has been used. The TGA has been carried out in air by means of a TGA 2950 V5.4A instrument in dynamic conditions using a heating rate 10 °C/min up to a maximum temperature of 1000 °C.

1.5 Electrochemical characterization: polarization curves

The electrochemical behavior of the coatings was also studied in order to test their possible corrosion protective properties. Potentiodynamic polarization curves were measured using a potentiostat/galvanostat Autolab PGSTAT 30. The samples were immersed in 100 mL of Dulbecco´s MEM (DMEM, Biochrom) at 37 °C. A conventional three electrode system was used, where a platinum foil served as counter electrode and Ag/AgCl (3 mol.dm^{-3} KCl) was used as reference electrode. The analysis was carried out using an O-ring cell with an exposed sample area of 0.38 cm^2. The potentiodynamic polarization was started at an absolute potential of – 1 V and the curves were measured up to 1 V with a potential sweep rate of 1 mV/s.

1.6 Simulate body fluid (SBF) bioactivity test

The coated samples have been subjected to *in vitro* bioactivity test in simulated body fluid (SBF). The SBF has ion concentrations almost equal to those of human blood plasma and it is buffered at pH 7.40 with 50 mM trishydroxymethylaminomethane and 45 mM hydrochloric acid at 36.5 °C, as reported in literature [8]. The test was performed by following the protocol of Kyoto University as suggested by the ISO standard [19], maintaining samples at 37 °C in 50 ml of SBF for 1, 2, 3, 5, 7, 14, 21 and 28 days, performing a refresh of the solution every 7 days. This bioactivity test is commonly used to predict the ability of bioactive materials to bond to leaving bone by detecting the precipitation of a hydroxyapatite (HAp) layer on their surface after soaking in SBF. The sample surface has been observed after different time points of immersion by Field Emission Scanning Electron Microscopy (FESEM, SUPRATM 40, Zeiss, Oberkochen, Germany) equipped with EDS.

1.7 Cytocompatibility evaluation

Biological experiments were carried on 1 cm diameter round specimens made of *i*) bulk stainless steel (SS), *ii*) SS coated with alginate (Alg) and *iii*) SS coated with 45S5_Zn/Alg. Specimens were sterilized by means of UV-light (30 minutes each side) and stored at room temperature protected from light until use.

1.7.1 Cells cultivation

Human primary fibroblasts (HGF) were purchased from the American Type Culture Collection (PCS-201-018 from ATCC, Manassas, USA) and cultivated in alpha-modified minimal essential medium (α-MEM, Sigma Aldrich, Milan, Italy) supplemented with 10% foetal bovine serum (FBS, Sigma Aldrich, Milan, Italy) and 1& antibiotics (penicillin/streptomycin) at 37 °C, 5% CO_2 atmosphere. Cells were cultivated until 80-90% confluence, enzymatically detached by trypsin-EDTA and used for experiments.

1.7.2 Indirect assay

Sterile specimens were located into a 24 multiwell plate and submerged by medium (1 ml/specimen); the plate was incubated at 37 °C for 1 week after that supernatants were collected and used to cultivated HGF cells. Accordingly, a defined number of cells ($7x10^3$/well) were seeded onto a 24 multiwell plate and cultivated with the collected supernatants; cells cultivated with supernatants collected from bulk SS specimens were considered as 100% control. Cells were cultivated for 1-3-7 days and at each time-point the viability was verified by means of metabolic activity using the colorimetric metabolic 3-(4,5-dimethylthiazol-2-yl)-2,5-diphenyltetrazolium bromide assay (MTT, Sigma-Aldrich, Milan, Italy). Briefly, the MTT solution (0.2 mg/ml) was added to each well and the plate was incubated at 37 °C 4 hours protected from light: then, the formazan crystals were solved with 100 μl of dimethyl sulfoxide (DMSO, Sigma-Aldrich, Milan, Italy) that were moved to a new 96 well plate. The optical density (o.d.) was measured with a spectrophotometer (Spark, from Tecan Group Ltd, Männedorf, Switzerland) using a 570 nm wavelength. Controls o.d. was considered as 100% and test specimens normalized towards it.

1.7.3 Direct assay

For the direct assay, HGF cells were directly drop-wised onto specimens' surface in a defined number ($7x10^3$ cells/specimen, 100 μl) and allowed to adhere 4 hours at 37 °C. Afterwards, specimens were fully submerged with 1 ml/well of fresh medium and cultivated for 1-3-7 days; at each time point, cells' viability was evaluated by the MTT assay as previously described.

1.7.4 Morphological evaluation

After 7 days of direct cultivation, cells morphology was checked by Field Emission Scanning Electron Microscopy (FESEM, SUPRATM 40, Zeiss, Oberkochen, Germany). Briefly, specimens were fixed at room temperature with formaldehyde (4% in PBS, 20 minutes), dehydrated by the alcohol scale (70-90-100%, 2 hours each) and cover sputtered with Cr. SEM was operated at different magnifications in order to visualize

cells adhesion and spread onto specimens' surface. Moreover, the ability of cells to correctly express their matrix onto specimens' surface was visually checked by means of fluorescence images of deposited type I collagen [20] by a Leica SP8 confocal platform (from Leica Microsystems, Wetzlar, Germany). Specimens were fixed 5 minutes at room temperature with 4% formaldehyde and then incubated with an anti-collagen type I antibody (ab34710 from AbCam, UK, 1:100 in PBS 1% bovine serum albumin, 5% goat serum) at 4°C overnight. The day after specimens were carefully washed with PBS to remove non-specific background and co-stained with 4′,6-diamidino-2-phenylindole (DAPI, from Sigma-Aldrich, 1:500 in PBS) and phalloidin (rhodamine B tetramethyl isothiocyanate, from AbCam, UK, 1:2000 in PBS) to visualize nuclei and cytoskeleton f-actins filaments, respectively.

1.7.5 Statistical analysis of data

Biological experiments were performed using 6 replicates. Samples were statistically compared by the SPSS software (v25, IBM) using the one-way ANOVA test after check of normal distribution and homogeneity using Shapiro-Wilk's and Levene's test respectively. Tukey's test was used for post-hoc analysis. Differences were considered as significant for $p<0.05$.

2. Results and discussion

2.1 Suspension stability via Zeta potential

It is well known that the water electrolysis during EPD can negatively affect the adhesion and the homogeneity of the coating, due to bubbles generation [21]. In order to avoid this problem and to promote a better stability of the mixture of polymer and glass particles, the suspension was prepared using a water-ethanol solution. Different water to ethanol ratios have been investigated and each of them present negative zeta potential, as reported in table 2, meaning an anodic deposition during EPD.

Water : ethanol mixture (vol.% each)	**Zeta potential [mV]**		
	45S5_Sr	**45S5_Zn**	**45S5_B**
100/0	-33 ± 5	-58 ± 6	-31 ± 7
80/20	-47 ± 9	-68 ± 8	-48 ± 7

60/40	-50 ± 12	-52 ± 11	-46 ± 12
40/60	-30 ± 15	-43 ± 13	-40 ± 16
20/80	-28 ± 14	-29 ± 13	-33 ± 13

Table 2: Zeta potential values of the 45S5_Sr, 45S5_Zn and 45S5_B glasses suspensions containing 2 g/L alginate for different water: ethanol ratios.

At 100 vol% water, the suspensions containing 45S5_Sr and 45S5_B present a reduced stability (around 30 mV). A reduced colloidal stability occurs also for the three suspensions at ethanol concentrations beyond 80 vol.%. An optimal zeta potential range for EPD has been obtained with ethanol concentrations of 20 and 40 vol.%. for each glass suspension (between -47 ± 9 and -68 ± 8 mV). In order to reduce the hydrogen evolution during deposition, a water: ethanol ratio of 60/40 was selected. The zeta potential of suspensions of glass powders without polymer was also measured as control (table 3), to understand the interaction between the glass particles and the alginate.

	Zeta potential [mv]
45S5_Sr 60/40 Water/ethanol	-24 ± 10
45S5_Zn 60/40 Water/ethanol	-41 ± 11
45S5_B 60/40 Water/ethanol	-21 ± 13

Table 3: Zeta potential measurements on pure glasses suspensions.

Comparing the results from table 2 and table 3, it can be affirmed that the suspension stability is controlled by alginate. For all suspensions, once alginate is added the zeta-potential nominal value increases 26, 11 and 25 mV for the 45S5_Sr/Alg, 45S5_Zn/Alg and 45S5_B/Alg, respectively, when compared to the suspension without alginate. The colloidal stabilization induced by alginate could be explained by two possible phenomena. The dissolved alginate drags the glass particles during the deposition, forming a kind of net the traps the glass particles. The second possibility is an interaction of the positive charges, from the different oxides, on the glass surface with the negative charges of the alginate molecule.

2.2 Deposition process

2.2.1 Mono-layer

In order to obtain homogeneous and crack-free coatings, different EPD cycles has been tried, changing parameters such as deposition time and potential. Generally, it has been noticed that a high potential value (>40 V) can induce the evolution of hydrogen and oxygen on the respective electrode surfaces due to reduction and oxidation of water from the electrolyte, which in turn caused the formation of bubbles. On the contrary, a low potential (< 10 V) produces very inhomogeneous, too thin coatings with lack of adhesion to the substrate. For each suspension the optimal deposition conditions have been determined: 30 V / 10 s for 45S5_Sr/Alg, 10 V / 30 s for 45S5_Zn/Alg and 20 V / 10 s for 45S5_B/Alg system. Figure 1a-c reports the morphology of the different coatings. As it can be observed the three coatings are very similar one to each other, being homogeneous and with a surface without bubbles or cracks.

2.2.2 Multi-layer

In order to increase the coating thickness meaning a higher glass amount, but avoiding the bubble formation induced by large deposition times, a multilayer approach, until 3 layers, was analyzed. The deposition parameters were maintained unaltered, introducing a drying step of 15 minutes at room conditions between each deposition.

Two layers have been prepared with the Sr and B doped glasses, three layers for Zn doped one (figure 1d-f). Figure 1e shows that the coating obtained with Zn-doped glass is highly uniform and bubble-free, while for the other two compositions (figure 1d and f) some inhomogeneities are present, particularly on the samples' edges, so a 3 layers coating seemed to be the best option.

2.3 Morphological, compositional and mechanical characterization

2.3.1 Coatings adhesion (qualitative bending test)

After the parameters optimization, on the best set of multilayered specimens, a bending test has been performed, in order to evaluate the coating adhesion. The coated samples have been folded as described in figure 2, put into distilled water in incubator at 37 °C for 24 hours, then removed from the solution, dried at room temperature and observed by optical microscopy in order to evaluate the eventual crack formation in the bended area and coating dissolution. As reported in figure 2, no sign of delamination or cracks is present in the area subjected to the maximum stress.

2.3.2 Coating morphology and composition

45S5_Sr/Alg coating

Figure 3 shows that the coatings cover the whole substrate surface. Moreover, the glass particles seem to be well embedded into the alginate matrix. Figure 3b and c show the detail of some glass powder cluster included into the polymer.

The cross section of 45S5_Sr/Alg 1 layer (figure 3g) evidences that the glass powders are completely embedded into the whole thickness of the coating, not only on its surface. The coating thickness, for one layer deposition, is around 2.3 μm.

45S5_Zn coating

Figure 4 shows the homogeneity of the coating: the substrate surface is well covered and no crack are visible. Due to the higher number of deposition steps the amount of glass particles is higher as well (figure 4d, e and f).

The cross section (figure 4g and h) shows the presence of three layers, with some discontinuities at the interface between the glass powders and the polymer. The thickness of the coating obtained with three depositions is about 25 μm.

45S5_B/Alg coating

Figure 5 shows the top view at different magnification of the mono- and bi-layer coatings with 45S5_B. In both cases, the coatings appear homogeneous with glass particles well embedded in the polymeric matrix.

2.3.3 Roughness and contact angle

The roughness measured on different coated samples, compared with the uncoated substrate, are reported in table 5. The data evidence that the roughness of each kind of coating is higher in respect to those of the uncoated samples, moreover all samples with multi-layered coatings shows a higher roughness, probably connected to the higher mass of deposited material. The wetting ability of each coating has been evaluated by contact angle measurements, as reported in table 5, where each value is the average of three different measures on the same sample. For each kind of coating, it can be observed a significant decrease of contact angle, correlated to the hydrophobic nature of the coating and an improved wettability compared to the bare substrate.

Property	Bare SS	45S5_Sr/Alg		45S5_Zn/Alg		45S5_B/Alg	
		1 layer	2 layers	1 layer	3 layers	1 layer	2 layers
Roughness (Ra / µm)	0.37±0.04	1.9 ± 0.3	3.2 ± 0.5	1.2 ± 0.3	1.9 ± 0.2	1.64 ± 0.08	1.8 ± 0.2
Contact angle	95,2	46 ± 6	30 ± 4	52 ± 8	22 ± 6	< 20	< 20

Table 5: Roughness and contact angle measurements

In these coatings the alginate shows an increase of hydrophilicity, due to the presence of –OH groups than interact with water molecules. This effect has been observed also in literature reporting the use of this polymer to increase surface hydrophilicity of various materials [22]. Additionally, the presence of glass particles into the coating can give a contribution to the hydrophilicity increase. The contact angle decreases as much as the EPD cycles number increases; this effect could be related to the porous morphology typical of multilayered coatings, which help the drop infiltration. It is worth of mentioning that a high surface roughness and hydrophilicity are positive characteristics to promote the cell adhesion and the fast formation of new bone tissue at the interface bone-implant in vivo [23]. For this reason, the wetting ability of the prepared coating seem promising for a good cell interaction.

2.3.4 Fourier-transform infrared spectroscopy (FTIR)

Figure 6 report the FTIR analysis performed on the composite coatings with 45S5_Sr, 45S5_Zn and 45S5_B. The presence of alginate is confirmed by the characteristic peaks of both asymmetric and symmetric stretching of COO^- group at 1600 cm^{-1} and 1423-1413 cm^{-1} respectively [7]. The patterns of glass powders show the peaks of asymmetric stretching of Si-O bond at 1050 cm^{-1} and those at 800 cm^{-1} due to bending of Si-O [7]. These results confirm the composite nature of the EPD coatings.

2.4 Thermogravimetric analysis

The thermogravimetric analyses showed a weight loss around 100 °C, that could be related to the loss of adsorbed H_2O, a second step above 250 °C ascribed to the thermal decomposition of alginate, that is reported in literature in the range between 170 and 500 °C [24]; above 550 °C a plateau can be observed, that could be related to the complete decomposition of alginate and the residual amount of glass.

Table 6 reports the percentages of polymer and glass contained in the different coatings. It can be noticed that the polymer is present in percentages between 23.2-25.4 % and the glass between 74.6-76.8%. Then, the polymer/glass ration is about 1:3, in agreement with the ratio of starting solution, meaning a successful tailoring of the coating by the suspension composition.

	Water [wt%]	**Polymer [wt%]**	**Glass [wt%]**	**Polymer [wt%]**	**Glass [wt%]**
Coating containing 45S5_Sr	8.4	22.7	68.9	24.8	75.2
Coating containing 45S5_Zn	7.7	21.4	7.09	23.2	76.8
Coating containing 45S5_B	8.4	23.3	68.3	25.4	74.6

Table 6: Obtained polymer/glass percentages in the coatings. In the right part of the table the percentages were re-calculated without considering the water content.

2.5 Electrochemical characterization

One of the potential functions of the investigated coatings is the possibility of protecting the metallic substrate from corrosion in contact with biological fluids, rich of chloride ions. Figure 7 shows the anodic polarization curves of the coated samples, compared with the curve registered on a sample of uncoated stainless steel AISI 316L. All the investigated samples show a lower corrosion current density than bare AISI 316L substrate, evidencing a slower degradation kinetics. All multilayer samples present a lower corrosion potential and larger corrosion current density than the single layer samples, this phenomenon may be related to a possible faster dissolution of the second layer. During the second layer deposition gas bubbles can be trapped between the two layers or lack of attachment can generate a space for electrolyte diffusion allowing a potential faster degradation of the second layer and a lower thermodynamical stability. This last aspect could be also the reason of the lower corrosion potential of the 45S5_B/Alg - 2 layers and 45S5_Sr/Alg – 2 layer samples compared to the bare substrate. Moreover, the polarization curves indicate remarkably reduced passive current densities in the anodic curves for all coated samples and no indication of breakdown of passivity at potentials < 1 V as observed for the bare stainless steel sample. Therefore, the here fabricated composite coatings offer good corrosion protection for the stainless steel surface in the chloride-containing environment of the simulated physiological electrolyte.

2.6 Simulated body fluid bioactivity test

Each sample was observed and analyzed via SEM/EDS to determine and characterize the growth of hydroxyapatite after soaking in SBF. Figure 8 shows as example the results of the morphological and chemical characterization on the surfaces of the different coatings after 7 and 28 days of immersion in SBF. In particular, for the coatings made with 45S5_Sr/alginate, after one and three days it was not possible to observe any hydroxyapatite precipitation. After 7 days of soaking in SBF (figure 8a,b) the surface morphology changes, and the EDS analysis shows the increase of Si (probably due to the condensation of silica gel), and the increase of P and Ca (due to HAp nucleation), in accordance with the bioactivity mechanism reported in literature, specifically with steps III and IV of it [8].

After 14 and 21 days of immersion in SBF also some particles with a morphology similar to HAp or its precursors was observed. EDS analysis shows the prevalence of Ca and P signals in respect to the Si one; this let suppose that the IV or V step of the bioactivity mechanism was reached. After 28 days of immersion in SBF (figure 8c,d) it is evident the presence of a phase rich in Ca and P, evidenced by the higher intensity of these element signals (EDS analysis).

The morphological and compositional analysis of 45S5_Zn/Alg coating after 7 and 28 days of immersion in SBF is reported in figures 8d-g. After 1 day of immersion no signs of HAp precipitation are observable. After 3 days of immersion a thin layer of HAp or its precursors are visible, and the EDS analysis shows an enrichment of Ca and P and a reduction of Si. However, this layer is not continuous and seems visible only in some particular areas. After 7 days the HAp layer seems thicker and the EDS analysis shows a significant increase of Ca and P, as a result of the formation of HAp or its precursors (figure 8e,f). After 21 and 28 days of immersion in SBF (figure 8g,h) the HAp layer covers the whole surface. The EDS analysis (figure 8h) shows peaks of high intensity for Ca and P. Moreover, the signals of Zn are still present, thus this element was not completely released during soaking in SBF up to 28 days. This feature is not in complete agreement with literature [25] and evidences that doping with Zn does not affect negatively the bioactivity of the glass.

The morphology and compositional analysis of the composite coatings 45S5_B/Alg after 7 and 28 days of soaking in SBF are reported in figure 8i-n. Also, in this case after 1 day of soaking any sign of HAp (nor precursors) precipitation is visible. After 3 days, the morphology of the surface shows the presence of cracks, typical of reaction layer growth from aqueous solutions. After 7 days of soaking in SBF the coating appears covered by HAp with the typical globular morphology (figure 8i) and confirmed by the compositional analysis by EDS (figure 8l). After 14 days of immersion a further enrichment of Ca and P content is observable and the surface shows the typical cauliflower morphology. After 21 and 28 days of immersion (figure 8m,n), the HAp

layer, with typical cauliflower morphology, is clearly visible on the whole surface. In conclusion each kind of coating shows a good level of bioactivity.

2.7 Biocompatibility test

2.7.1 Specimens' cytocompatibility

After chemical-physical characterization, specimens were tested for their cytocompatibility *in vitro* towards fibroblasts, due to the evidence that such cells are usually the first to migrate to the implanted device thus favoring scaffold colonization [26, 27]. In fact, if fibroblasts do not well-integrate with the foreign body, a pro-inflammatory cascade is often activated involving the secretion of chemokines IL6, IL8, and monocyte chemoattractant protein 1 (MCP1) [28]. The selected specimens for biological tests were i) bulk stainless steel (SS), ii) SS coated with alginate (Alg) and iii) SS coated with Alg-45S5_Zn due to the demonstrated cytocompatibility of the first two [29, 30] and the potential toxic effect of the of the last caused by zinc. In fact, despite Zn is known to be a cytocompatible [31], antibacterial [32] and pro-regenerative [33] trace element, some literature reported about toxic side effects mostly related to the released amount [34]. Accordingly, specimens were firstly tested in a not direct assay where they were immersed in culture media for 7 days at 37 °C in order to make them release the potential toxic elements. Afterwards, the such pre-treated media were used to cultivate cells to evaluate any toxic effect. Results are reported in figure 9a. None of the tested specimens caused a significant decrease of cells metabolism in comparison to the bulk SS control ($p>0.05$, all results >85%) thus demonstrating the lack of toxic elements released in the medium during the pre-incubation 7 day period.

Despite the promising results obtained by the not direct assay, it must be considered that such evaluation is not representative for the fitting of the cells to the specimens' surface properties that can influence cells' fate according to many parameters such as the topography, surface energy, wettability etc. So, a direct assay was performed by directly seeding the cells onto specimens' surface. Results are reported in figure 9b. After 1-day cultivation, cells cultivated onto alg-45S5_Zn specimens reported a significant reduction of their metabolic activity in comparison with both bulk SS and Alg ones ($p<0.05$, indicated by the *) thus suggesting for a toxic effect (≈60% of viable cells). However, in the following 2- and 3-day cultivation the values increased up to ≈80% (day 2) and >90% (day 3) being not significant towards bulk SS and Alg specimens ($p>0.05$). Therefore, the initial value related to 1-day cultivation was revalued as a greater difficulty for the cells to adapt to the surface in comparison to the bulk SS and Alg rather than an intrinsic toxic effect exploited by the Zn. As a

confirmation of this hypothesis, both fluorescence (figure 9c) and SEM images (figure 9d-e) relative to day 7 cultivation revealed that cells correctly adhered and spread onto the test surfaces as well as they expressed collagen considered as matrix marker. Here, alginate was considered as the comparison for the Alg-45S5_Zn specimens due to the best results obtained in the direct evaluation assay and due to its well-known ability in promoting fibroblasts adhesion and migration for tissue engineering purposes as recently demonstrated for example by Lueckgen et al. [35]. Fluorescent images demonstrated that cells density and morphology were comparable between Alg and alg-45S5_Zn as demonstrated by the number of stained nuclei (DAPI) and the elongated spread evaluated by f-actin filaments (phalloidin). Thanks to these “cells friendly” properties displayed by both the two coatings, the majority of cells were found to expressed type I collagen being so well integrated with the specimens’ surface. Cells’ adaption to the specimens’ surface was further demonstrated by SEM images (figure 9d-e). In fact, while the lower magnification images (left panels) showed cells spreading onto specimens’ surface, the higher magnification ones (right panels) displayed the presence of filopodia. This is a fundamental step for the successful device repopulation upon implant as cell’s movement starts with the filopodia attachment via integrins and continue when the cell cytoskeleton contraction breaks the cell-matrix anchorage thus allowing the cell moving forward [36]; by this way, fibroblast start to colonize the implanted device, kicking off to the self-repair process.

Conclusions

The aim of this work was the realization through EPD of composite coatings with sodium alginate matrix containing particles of three different bioactive glasses, doped respectively with Sr, Zn and B oxides. The parameters of the EPD process have been optimized during several anodic EPD cycles and the coatings characterized by means of morphological and compositional viewpoints, as well as for their bioactivity and biocompatibility. All kinds of coatings showed good homogeneity and high resistance to deformation. The corrosion test revealed a protective behavior for each kind of composite coating. The thermogravimetric analysis showed that the percentages of glass and polymer are constant before and after the deposition. All coating showed a bioactive behavior, even if with different kinetics: the coatings containing 45S5_Zn glass evidenced the fastest bioactivity mechanism. The biocompatibility test of 45S5_Zn/Alg coatings demonstrated an initial reduction of cell viability; however, after 48-72 hours cells were able to proliferate on the samples surface and to produce collagen from the ECM. Due to the obtained results, the developed coatings are promising candidates to impart biological activity to metallic substrates for bone contacting materials in orthopedic applications.

References

[1] A.R. Boccaccini, S. Keim, R. Ma, Y. Li, I. Zhitomirsky, Electrophoretic deposition of biomaterials. J. R. Soc. Interface. 7 (5) (2010) 581-613. doi: 10.1098/rsif.2010.0156.focus.

[2] R. Ma and I. Zhitomirsky, Electrophoretic deposition of silica–hyaluronic acid and titania–hyaluronic acid nanocomposites, J. Alloys and Compounds 509 (2011) S510–S513. Doi:10.1016/j.jallcom.2010.10.111

[3] A. R. Boccaccini, C. Peters, J. A. Roether, D. Eifler, S. K. Misra, E. J. Minay, Electrophoretic deposition of polyetheretherketone (PEEK) and PEEK/Bioglass® coatings on NiTi shape memory alloy wires, J. Mater. Sci. 41 (2006) 8152-8159. Doi:10.1007/s10853-006-0556-z

[4] M. Miola, E. Verné, F. E. Ciraldo, L. Cordero-Arias, A.R. Boccaccini, Electrophoretic Deposition of Chitosan/45S5 Bioactive Glass Composite Coatings Doped with Zn and Sr. Frontiers In Bioengineering And Biotechnology 3(2015). Doi:10.3389/fbioe.2015.00159

[5] M. Miola, E. Verné, A. Piredda, S. Seuss, S. Cabanas-Polo, A.R. Boccaccini, Development and Characterization of PEEK/B2O3-Doped 45S5 Bioactive Glass Composite Coatings Obtained by Electrophoretic Deposition. Key Engineering Materials 654(2015), 165-169. Doi:10.4028/www.scientific.net/KEM.654.165

[6] Q. Chen, L. Cordero-Arias J. A Roether, S. Cabanas-Polo, S. Virtanen, A. R. Boccaccini, Alginate/Bioglass® composite coatings on stainless steel deposited by direct current and alternating current electrophoretic deposition, Surf. Coat. Technol. 233 (2013) 49–56. Doi:10.1016/j.surfcoat.2013.01.042

[7] L. Cordero-Arias, S. Cabanas-Polo, J. Gilabert,O. M. Goudouri, E. Sanchez, S. Virtanen, A. R. Boccaccini, Electrophoretic deposition of nanostructured TiO2/alginate and TiO2-bioactive glass/alginate composite coatings on stainless steel .Advances in Applied Ceramics Structural, Functional and Bioceramics 113 (2014) 42-49. doi:10.1179/1743676113Y.0000000096

[8] T. Kokubo and H. Takadama, “How useful is SBF in predicting in vivo bone bioactivity?” Biomat. 27 (2006) 2907–2915. Doi:10.1016/j.biomaterials.2006.01.017

[9] L.L. Hench, Bioceramics. J. Am. Ceram. Soc. 81 (1998) 1705–1728. Doi:10.1111/j.1151-2916.1998.tb02540.x

[10] A. Hoppe, N.S. Güldal, A.R. Boccaccini. A review of the biological response to ionic dissolution products from bioactive glasses and glass-ceramics. Biomaterials 32(11) (2011) 2757-2774. Doi:10.1016/j.biomaterials.2011.01.004

[11] A. A. Gorustovich, J. M. Porto Lopez, M. B. Guglielmotti, R. L. Cabrini. Biological performance of boron-modified bioactive glass particles implanted in rat tibia bone marrow. Biomed. Mater. 1 (2006) 100–105. DOI: 10.1088/1748-6041/1/3/002

[12] L. A. Haro Durand, A. Góngora, J. M. Porto López, A. R. Boccaccini, P. Zago, A. Baldi, A. A. Gorustovich, In vitro endothelial cell response to ionic dissolution products from boron-doped bioactive glass in the SiO2-CaO-P2O5-Na2O system, J. Mater. Chem. B 2 (2014) 7620-7630. Doi:10.1039/C4TB01043D

[13] M. Yamaguchi. Role of zinc in bone formation and bone resorption. J. Trace Elem. Exp. Med. 11(2e3) (1998) 119-135. Doi:10.1002/(SICI)1520-670X(1998)11:2/3<119::AID-JTRA5>3.0.CO;2-3

[14] I.S. Kwun, Y.E. Cho, R.AR Lomeda, H.I. Shin, J.Y. Choi, Y.H. Kang, et al. Zinc deficiency suppresses matrix mineralization and retards osteogenesis transiently with catch-up possibly through Runx 2 modulation. Bone 46(3) (2010) 732-741. DOI: 10.1016/j.bone.2009.11.003

[15] P.J. Marie, P. Ammann, G. Boivin, C. Rey. Mechanisms of action and therapeutic potential of strontium in bone. Calcif. Tissue Int. 69(3) (2001) 121-129. DOI: 10.1007/s002230010055

[16] B. Habermann, K. Kafchitsas, G. Olender, P. Augat, A. Kurth Strontium ranelate enhances callus strength more than PTH 1-34 in an osteoporotic rat model of fracture healing. Calcif. Tissue Int.86(1) (2010) 82-89. DOI: 10.1007/s00223-009-9317-8

[17] J. Sun, H, Tan, Alginate-Based Biomaterials for Regenerative Medicine applications Materials (Basel). 6(4) (2013) 1285–1309. DOI: 10.3390/ma6041285

[18] K. Yong Lee, D.J. Mooney, Alginate: properties and biomedical applications Prog Polym Sci. 37(1) (2012) 106–126. Doi:10.1016/j.progpolymsci.2011.06.003

[19] ISO 23317:2014, Implants for surgery — In vitro evaluation for apatite-forming ability of implant materials.

[20] S. Ferraris, A. Cochis, M. Cazzola, M. Tortello, A. Scalia, S. Spriano, L. Rimondini, Cytocompatible and anti-bacterial adhesion nanotextured titanium oxide layer on titanium surfaces for dental and orthopedic implants. Frontiers in bioengineering and biotechnology 7 (2019) 103. doi: 10.3389/fbioe.2019.00103

[21] L. Besra, M. Liu, A review on fundamentals and applications of electrophoretic deposit Progress in Materials Science 52(1) (2007) 1-61. Doi:10.1016/j.pmatsci.2006.07.001

[22] L.E. Cordero Arias, “Electrophoretic deposition of organic/inorganic composite coatings on metallic substrates for bone replacement applications: mechanisms and development of new bioactive materials based on polysaccharides”. Dissertation, University of Erlangen-Nuremberg (2015).

[23] B.D. Boyan, E.M. Lotz , Z.Schwartz. Roughness and Hydrophilicity as Osteogenic Biomimetic Surface Properties Tissue Eng Part A. 23(23-24) (2017) 1479-1489. doi: 10.1089/ten.TEA.2017.0048.

[24] J. P. Soares, J. E. Santos, G. O. Chierice,E. T. G. Cavalheiro, Thermal behavior of alginic acid and its sodium salt, Ecl. Quím., São Paulo, 29(2) (2004) 53-56. Doi:10.1590/S0100-46702004000200009

[25] H. Oudadesse, E. Dietrich, Y. Le Gal, P. Pellen, B. Bureau, A.A. Mostafa, G. Cathelineau, Apatite forming ability and cytocompatibility of pure and Zn-doped bioactive glasses, Biomed Mater. 6 (2011) 11-17. DOI: 10.1088/1748-6041/6/3/035006

[26] A. Cochis, S. Ferraris, R. Sorrentino, B. Azzimonti, C. Novara, F. Geobaldo, F. Truffa Giachet, C. Vineis, A. Varesano, A. Sayed Abdelgeliel, S. Spriano, L. Rimondini. Silver-doped keratin nanofibers preserve a titanium surface from biofilm contamination and favor soft-tissue healing. Journal of Materials Chemistry B, 5(42) (2017) 8366-8377. Doi:10.1039/C7TB01965C

[27] S. Ferraris, F.T. Giachet, M. Miola, E. Bertone, A. Varesano, C. Vineis, A. Cochis, R. Sorrentino, L. Rimondini, Spriano, S. Nanogrooves and keratin nanofibers on titanium surfaces aimed at driving gingival fibroblasts alignment and proliferation without increasing bacterial adhesion. Materials Science and Engineering: C, 76 (2017). 1-12. Doi:10.1016/j.msec.2017.02.152

[28] S. Bordin, T.F. Flemmig, M.D. Habil, S. Verardi, Role of fibroblast populations in peri-implantitis. International Journal of Oral & Maxillofacial Implants, 24(2) (2009) 197-204.

[29] D.O. Meredith, L. Eschbach, M.A. Wood, M.O. Riehle, A.S. Curtis, R.G. Richards. Human fibroblast reactions to standard and electropolished titanium and Ti–6Al–7Nb, and electropolished stainless steel. Journal of Biomedical Materials Research Part A 75(3) (2005) 541-555. DOI: 10.1002/jbm.a.30457

[30] R. Silva, R. Singh, B. Sarker, D.G. Papageorgiou, J.A. Juhasz-Bortuzzo, J.A. Roether, I. Cicha, J. Kaschta, D.W. Schubert, K. Chrissafis, R. Detsch, A.R. Boccaccini. Hydrogel matrices based on elastin and alginate for tissue engineering applications. International journal of biological macromolecules, 114 (2018) 614-625. Doi:10.1016/j.ijbiomac.2018.03.091

[31] Y. Su, K. Wang, J. Gao, Y. Yang, Y.X. Qin, Y. Zheng, D. Zhu, Enhanced cytocompatibility and antibacterial property of zinc phosphate coating on biodegradable zinc materials. Acta biomaterialia, 98 (2019) 174-185. Doi:10.1016/j.actbio.2019.03.055

[32] G.V. Vimbela, S.M. Ngo, C. Fraze, L. Yang, D.A. Stout, Antibacterial properties and toxicity from metallic nanomaterials. International journal of nanomedicine, 12,(2017) 3941-3965. DOI: 10.2147/IJN.S134526

[33] S. Kogan, A. Sood, M.S. Garnick, Zinc and wound healing: a review of zinc physiology and clinical applications. Wounds: a compendium of clinical research and practice, 29(4) (2017) 102-106.

[34] D. Hernández-Escobar, S. Champagne, H. Yilmazer, B. Dikici, C.J. Boehlert, H. Hermawan, Current status and perspectives of zinc-based absorbable alloys for biomedical applications. Acta Biomaterialia, 97 (2019) 1-22. Doi:10.1016/j.actbio.2019.07.034

[35] A. Lueckgen, D.S. Garske, A. Ellinghaus, D.J. Mooney, G.N. Duda, A. Cipitria, Enzymatically-degradable alginate hydrogels promote cell spreading and in vivo tissue infiltration. Biomaterials, 217 (2019) 119294. doi:10.1016/j.biomaterials.2019.119294

[36] C.D. Hartman, B.C. Isenberg, S.G. Chua, J.Y. Wong, Vascular smooth muscle cell durotaxis depends on extracellular matrix composition. Proceedings of the National Academy of Sciences, 113(40) (2016) 11190-11195. Doi:10.1073/pnas.1611324113

Figure captions:

Figure 1: Mono-layer coatings morphology: a) 45S5_Sr/Alg (30 V, 10 s), b) 45S5_Zn/Alg (10 V, 30 s), c) 45S5_B/Alg (20 V, 10 s) deposited from a 60 vol.% water and 40 vol.% EtOH suspension containing 2 g/L alginate and 6 g/L of the respective type of glass. Multi-layer coatings morphology: d) 45S5_Sr/Alg 2 layers, e) 45S5_Zn/Alg 3 layers, f) 45S5_B/Alg 2 layers.

Figure 2: Qualitative bending test results of a) 45S5_Sr/Alg coating, b) 45S5_Zn/Alg 3 layer coating, c) 45S5_B/Alg coating.

Figure 3: SEM micrographs of a-c) 45S5_Sr/Alg 1 layer, d-f) 45S5_Sr/Alg 2 layers, g) cross section of 45S5_Sr/Alg 1 layer

Figure 4: SEM micrographs of a-c) 45S5_Zn/Alg 1 layer, d-f) 45S5_Zn/Alg 3 layers, cross section of 45S5_Zn/Alg (3 layers) at g) low and h) high magnification.

Figure 5: SEM micrographs of a-c) 45S5_B/Alg 1 layer, d-f) 45S5_B/Alg 2 layers.

Figure 6: FTIR spectra of 45S5_Sr/Alg (A), 45S5_Zn/Alg (B) and 45S5_B/Alg (C) containing samples.

Figure 7: anodic polarization curves of the coated samples, compared with the curve of uncoated stainless steel AISI 316L.

Figure 8: SEM-EDS analysis of 45S5_Zn/Alg coatings after 7 (a,b – e,f – I,l) and 28 (c,d – g,h – m,n) days of immersion in SBF solution

Figure 9. Cytocompatibility evaluation. The not direct assay (a) revealed that no toxic compounds were released from the coatings in a 7-days pre-incubation period as no significant differences were noticed between groups ($p>0.05$). The direct assay (b) suggested that cells require more time to adapt to the Alg-45S5_Zn surface as a significant difference was noticed after 1 day ($p<0.05$, indicated by *) but not in the following time-points. Finally, after 7 days cultivation fluorescence staining (c) showed the presence of matrix collagen for all the coating, thus suggesting a successful fitting that was confirmed by the presence of filopodia observed revealed by the SEM images (d-e, right panels).

Figure 1

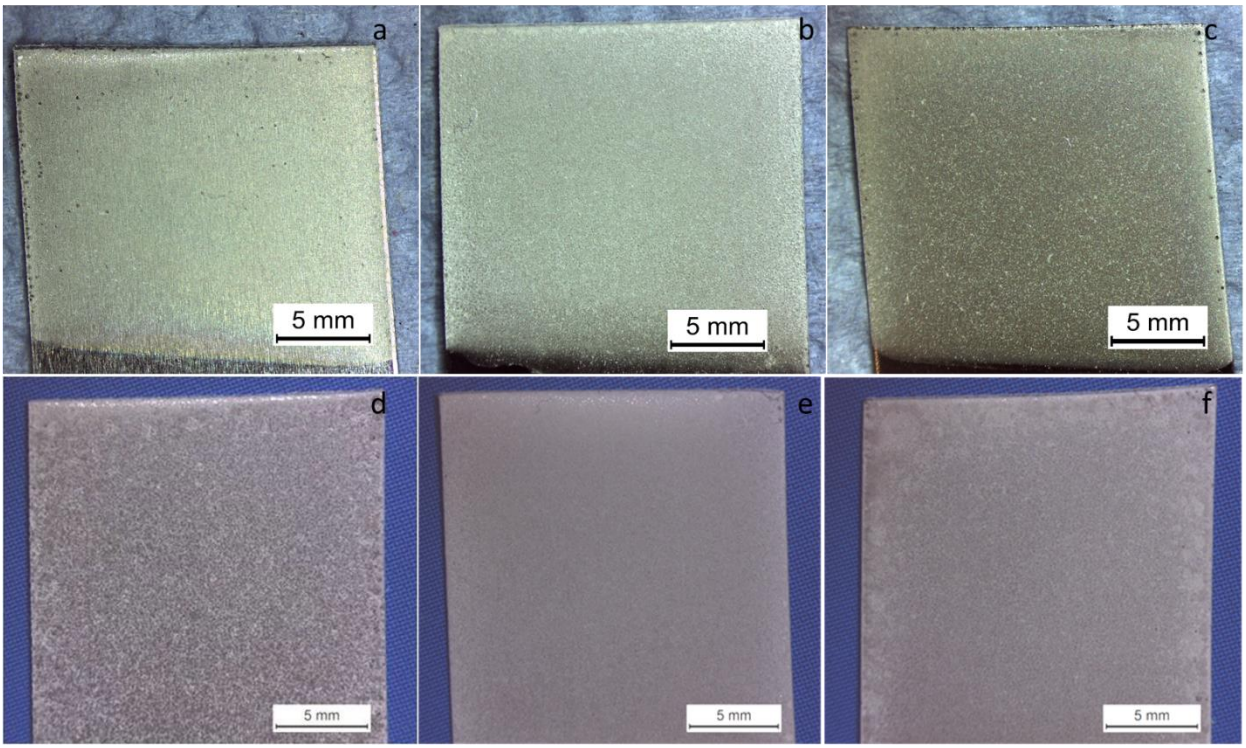

Figure 2

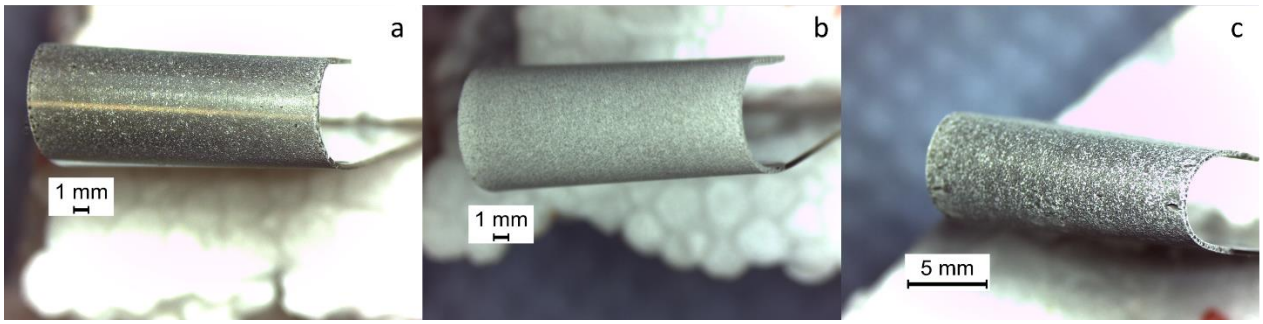

Figure 3

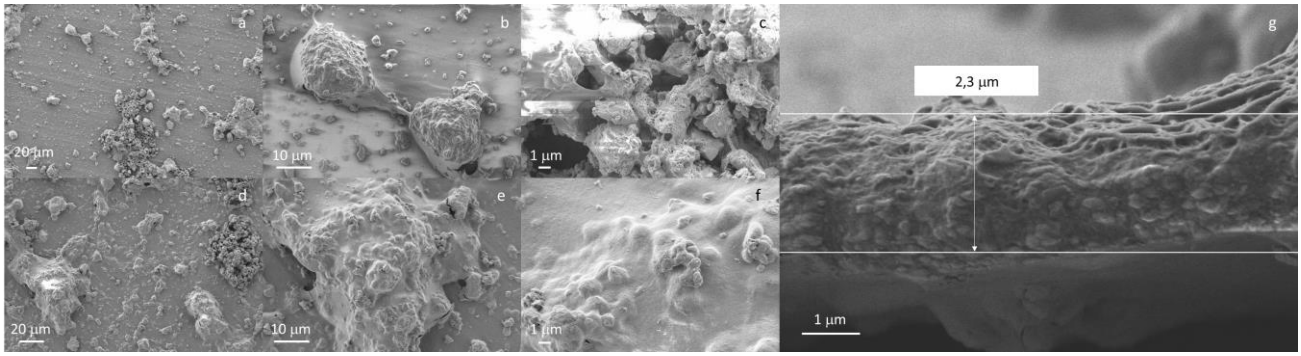

Figure 4

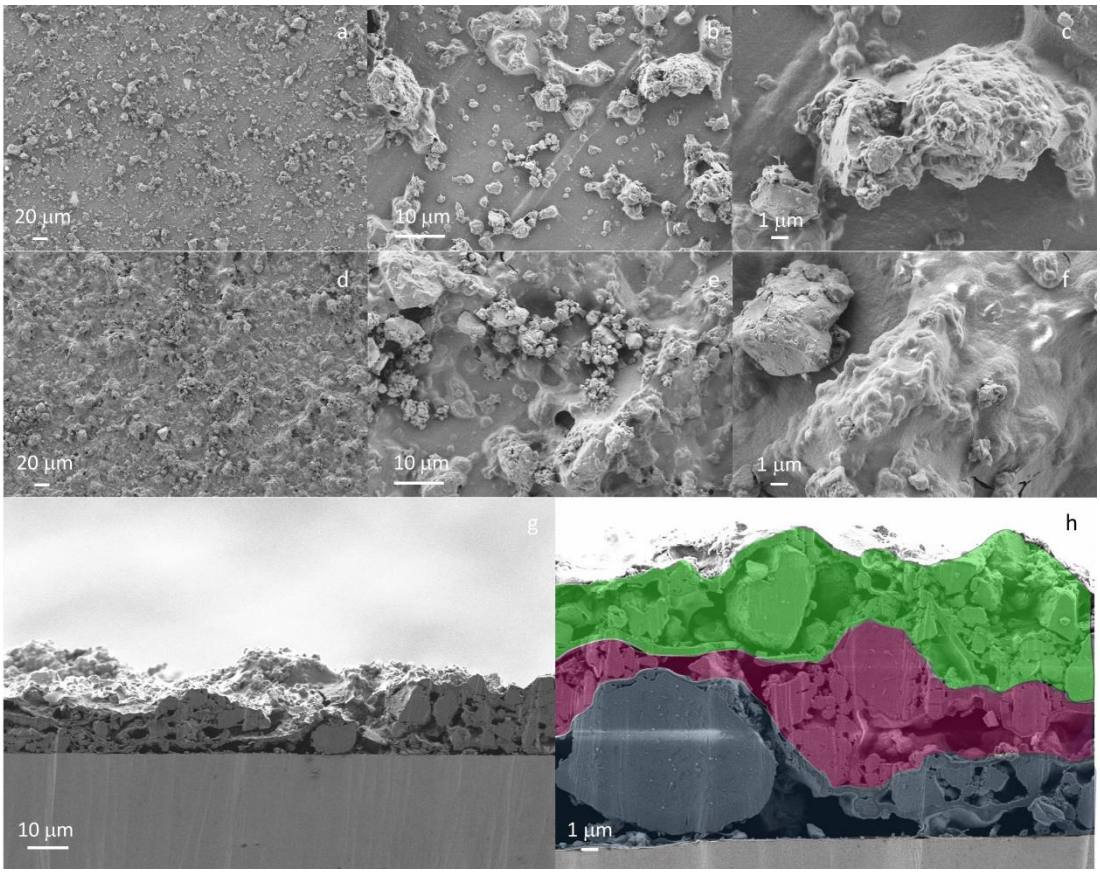

Figure 5

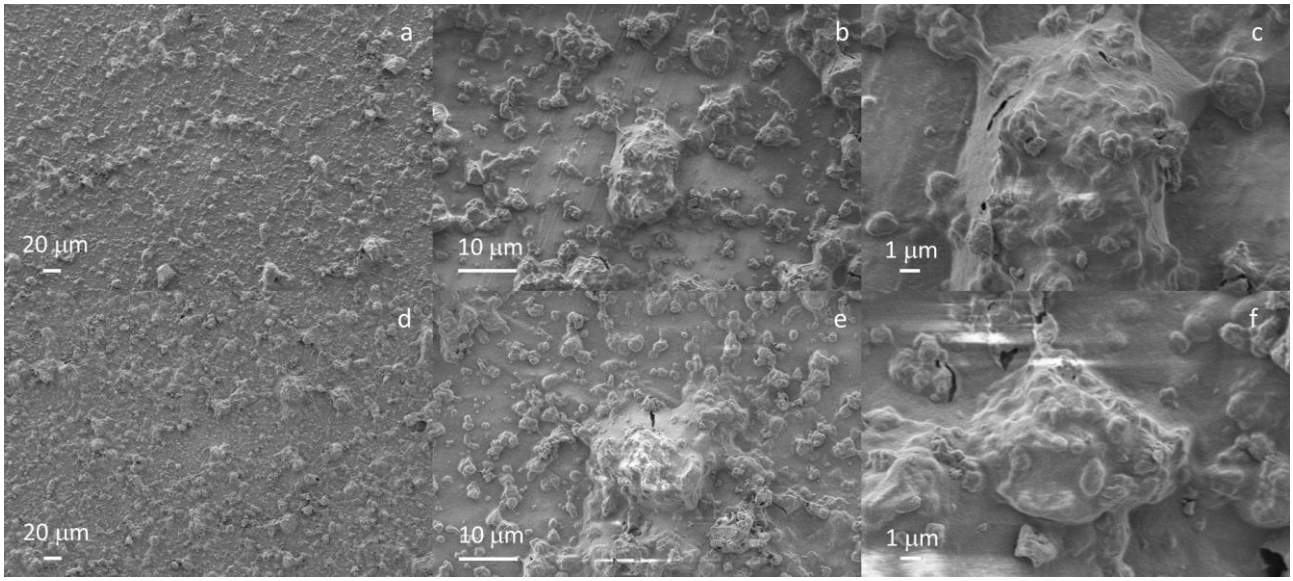

Figure 6

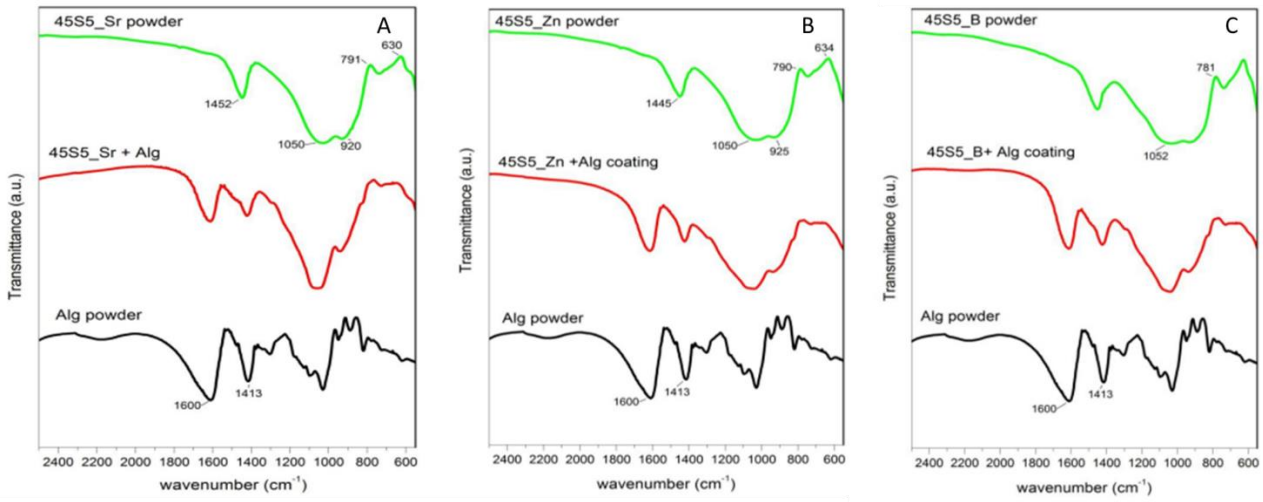
45S5_Sr powder
A
630
791
1452
1050
920
45S5_Sr + Alg
Alg powder
1600
1413
Transmittance (a.u.)
2400 2200 2000 1800 1600 1400 1200 1000 800 600
wavenumber (cm-1)
45S5_Zn powder
B
634
790
1445
1050
925
45S5_Zn +Alg coating
Alg powder
1600
1413
Transmittance (a.u.)
2400 2200 2000 1800 1600 1400 1200 1000 800 600
wavenumber (cm-1)
45S5_B powder
C
781
1052
45S5_B+ Alg coating
Alg powder
1600
1413
Transmittance (a.u.)
2400 2200 2000 1800 1600 1400 1200 1000 800 600
wavenumber (cm-1)

Figure 7

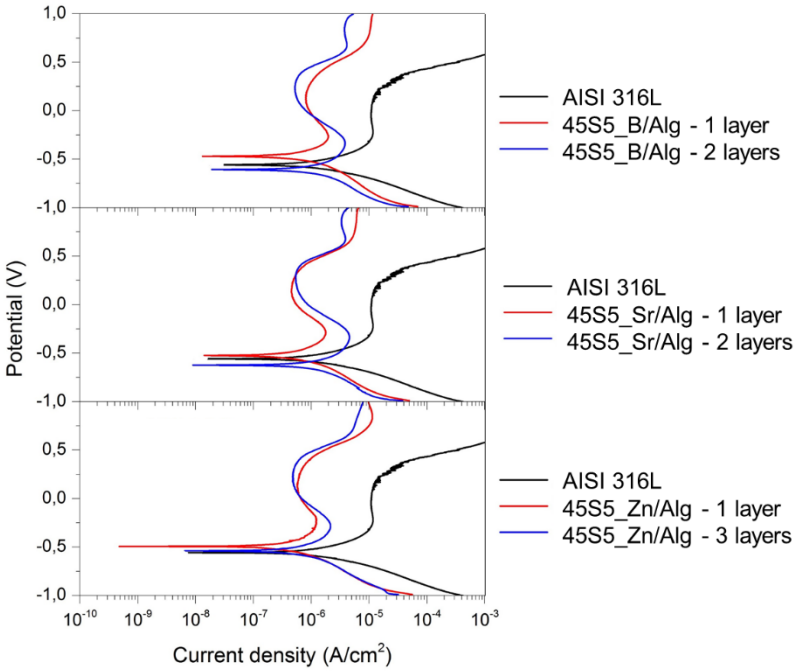
Potential (V)
1,0
0,5
0,0
-0,5
-1,0
Current density (A/cm^2)
10^{-10} 10^{-9} 10^{-8} 10^{-7} 10^{-6} 10^{-5} 10^{-4} 10^{-3}
AISI 316L
45S5_B/Alg - 1 layer
45S5_B/Alg - 2 layers
AISI 316L
45S5_Sr/Alg - 1 layer
45S5_Sr/Alg - 2 layers
AISI 316L
45S5_Zn/Alg - 1 layer
45S5_Zn/Alg - 3 layers

Figure 8

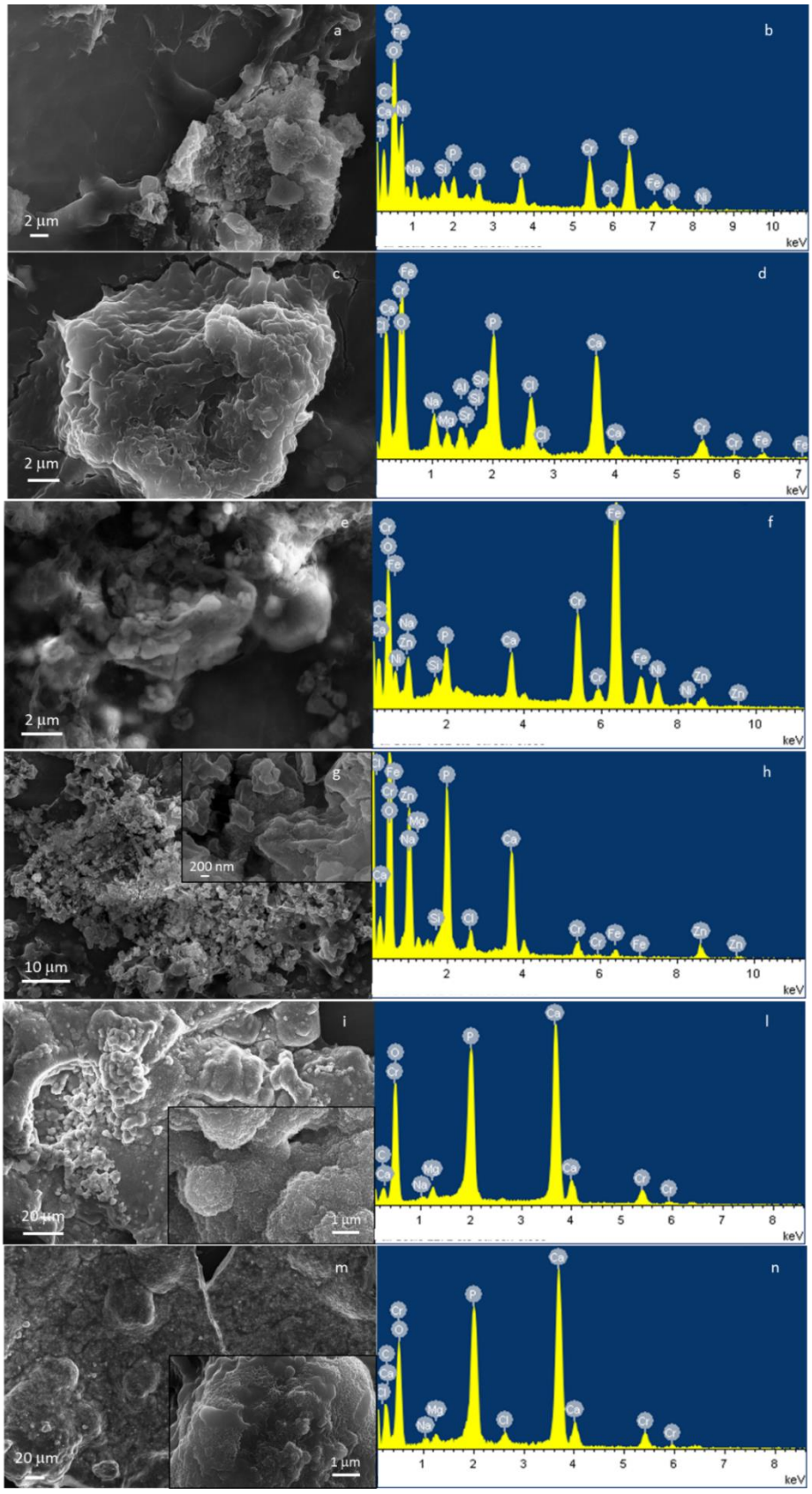
a
2 µm
b
keV
c
2 µm
d
keV
e
2 µm
f
keV
g
200 nm
10 µm
h
keV
i
20 µm
1 µm
l
keV
m
20 µm
1 µm
n
keV

Figure 9

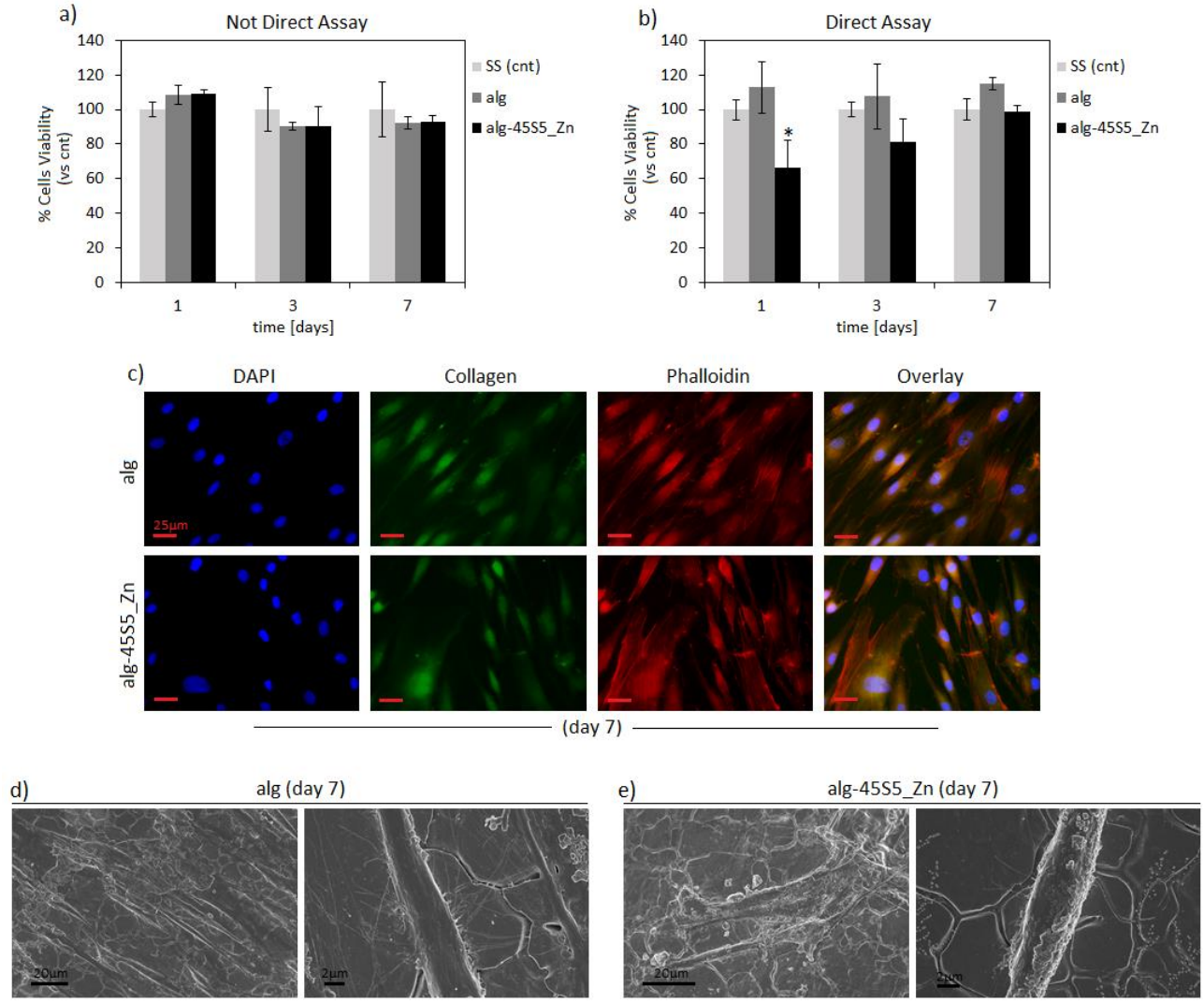
a)
Not Direct Assay
% Cells Viability (vs cnt)
time [days]
SS (cnt)
alg
alg-45S5_Zn
b)
Direct Assay
*
c)
DAPI
Collagen
Phalloidin
Overlay
alg
alg-45S5_Zn
25µm
(day 7)
d)
alg (day 7)
20µm
2µm
e)
alg-45S5_Zn (day 7)
20µm